Controlling the size and shape of Mg-MOF-74 crystals to optimise film synthesis on alumina substrates

James Campbell, Begum Tokay*

Advanced Materials Research Group, Chemical and Environmental Engineering Department, Faculty of Engineering, University of Nottingham, Nottingham, NG7 2RD, UK

Keywords: *Metal Organic Frameworks, Thin Films, Mg-MOF-74 membranes, CPO-27, Alumina Substrates, Membrane Synthesis, CO_2/CH_4 separation*

Abstract

Mg-MOF-74 is a metal organic framework with the highest CO_2 adsorption capacity of any porous material. Therefore, it has been suggested for CO_2 separations as both an adsorbent and incorporated into membranes. Design of the Mg-MOF-74 crystal morphology is important to expand the applicability of the material. In this paper one step synthesis of Mg-MOF-74 films has been achieved by controlling the Mg-MOF-74 crystal morphology. Results show that increasing the fraction of ethanol and water in the reaction solution relative to dimethyl formamide (DMF) increases the size of the crystals produced, while resulting in a subsequent drop in yield. By using solvent composition to control the Mg-MOF-74 crystal size and shape the synthesis of Mg-MOF-74 thin films was achieved in one step, without the need for seeding. Films could be produced as thin as 1 µm, ten times thinner than any other previous membranes in the M-MOF-74 series, in a fraction of the time (only 2.5 hours). Thicker films (up to 14 µm) could also be produced by increasing the fraction of ethanol and water in reaction solution, offering a methodology by which the thickness of Mg-MOF-74 membranes can be controlled. Films were produced on porous tubular alumina supports, and single gas measurements were conducted resulting in a CO_2 permeance of 7.4 x10^{-7} mol m^{-2} s^{-1} Pa^{-1} and an ideal CO_2/CH_4 selectivity of 0.5.

Keywords: Metal Organic Frameworks; Thin Films; Mg-MOF-74; CPO-27; Membrane Synthesis

1. Introduction

Metal organic frameworks (MOFs) are crystalline compounds consisting of metal ions connected by organic ligands[1]. The range of possible MOF structures available, due to the wide choice in ligands and metal ions[2], means MOFs can be specifically tailored to a number of applications. This ability to fabricate MOFs with specific pore sizes and tuneable sorption behaviours make them desirable for separations[3]. In order to maximise the potential of MOF materials, the morphological properties of the crystals must also be considered. Control of MOF crystal size and shape is an important parameter effecting the performance of MOFs as adsorbents[4,5] and filler particles in mixed matrix membranes (MMMs)[6–9]. Optimising MOF crystal shape is also imperative to produce the well intergrown films required to fabricate membranes for gas separations[2].

Membranes comprised of pure MOF films (e.g. ZIF-8[10–12], MOF-5[13], HKUST-1[14,15] etc[16–19]) on porous substrates with a clear, definitive MOF layer have been applied to gas separations, overcoming some of the issues associate with MMMs[3]. Typically, these membranes require long syntheses times and multiple steps to produce defect free barriers. Each MOF relies on

a unique synthesis methodology and control over the membrane properties, such as thickness and crystal orientation, is limited. These membranes have often only been grown on small flat disc substrates, with a limited surface area. Therefore their suitability for industrial processes is yet to be verified. Finding facile methodologies to fabricate MOF membranes with controllable morphologies would improve the applicability of MOF membrane technology to commercial operations.

The M-MOF-74 series (where M represents a metal ion such as Ni^{2+}) has garnered sizable research interest due to high CO_2 uptakes during adsorption[20–22]. The magnesium based Mg-MOF-74 has demonstrated the highest CO_2 uptake at low to moderate pressures of any solid adsorbent[23]. Mg-MOF-74 powder has been used to remove CO_2 selectively from flue gas (N_2) streams [24,25] and separate CO_2/CH_4 mixtures[26–28] via adsorption. However, research into the fabrication of M-MOF-74 membranes is so far limited.

Films of various M-MOF-74 species, including Mg-MOF-74, were grown on non-porous alumina substrates via direct growth by Betard *et al.*[29]. However, the film synthesis required a two-step process over 44 hours, resulting in films over 10 µm thick. They did not test these films as membranes for separations, but demonstrated synthesis methodologies to fabricate films from the M-MOF-74 series. Currently only two studies on the fabrication and testing of M-MOF-74 membranes have been published. In the first, Lee *et al*. used layer-by-layer seeding, followed by secondary growth to produce Ni-MOF-74 membranes on flat disc α-alumina substrates for range of gas separations such as H_2, CO_2, N_2 and CH_4[30]. The films required 72 hours of synthesis, resulting in membranes between 10 and 25 µm thick. In second Mg-MOF-74 membranes were synthesised via seeding and secondary growth, using MgO particles as nucleation sites on flat disc alumina supports and tested for H_2/CO_2 separations[31]. The subsequent films were fabricated over 24 hours and were 10 µm thick.

In order to reduce membrane thickness to ~1-2 µm and thus increase gas permeance, we suggest controlling the crystal grain size of the films. Methodologies developed to crystal size control including microwave and ultrasonic syntheses[21,22,32] and room temperature precipitation. The size of Zn-MOF-74 crystals were altered by changing the water/ethanol ratio of a reaction solution containing a sodium hydroxide additive in a solvothermal synthesis, with crystal sizes of 1 and 5 µm obtained[33]. Changing the solvent ratios of Mg-MOF-74 synthesis solutions offers a facile methodology to produce crystals of different sizes, and thus reducing the thickness of the films below that of other reported.

In the current study, we present a rapid fabrication methodology for Mg-MOF-74 films as thin as 1 µm on tubular alumina substrates via one-step synthesis. The choice of tubular supports allows for the high surface area to volume ratios required for industrial separations. The growth of MOFs on modular supports such as tubular supports[34] and hollow fibres[35–37] has previously been demonstrated for ZIF-8 and UiO-66 but not for any of the M-MOF-74 series. We controlled the size of Mg-MOF-74 crystals via the addition of ethanol and water to synthesis solutions. Rapid synthesis was achieved by using elevated temperatures and high reagent concentrations. The crystal synthesis methodology was then adapted to produce Mg-MOF-74 membranes on alumina substrates. This paper presents the first reported research on the fabrication of M-MOF-74 films with controllable thickness in a rapid, one step process.

2. Experimental

2.1 Materials

Magnesium acetate tetrahydrate ($Mg(CH_3COO)_2{\cdot}4H_2O$) (99%) and 2,5-dihydroxyterephthalic acid (H_4DHTP) (98%) were purchased from Sigma-Aldrich. Solvents, for synthesis and activation, dimethylformamide (DMF, 99.98%), ethanol (99.99%) and methanol (99.99%) were obtained from Fisher Scientific UK Ltd.

2.2 Mg-MOF-74 Crystal Synthesis

Mg-MOF-74 crystal synthesis was based on the previously reported method by Díaz-García et al.[38] with an elevated temperature to reduce synthesis time. In a typical synthesis, 0.39 to 0.41 g H_4DHTP was dissolved in 10 ml DMF using a magnetic stirrer until the ligand had completely dissolved. Metal salt solutions were prepared by complete dissolution of between 1.15 to 1.21 g magnesium acetate tetrahydrate in a 10 ml mixture of DMF, water and ethanol. The solvent volumes were altered depending on the desired crystal size. The solvent ratios used for each synthesis formulation are shown in **Table 1**.

Table 1: Solvent volumes used for synthesis to produce Mg-MOF-74 crystals and films

Solvent formulation	DMF: Water: Ethanol Volumes (ml)
F1	20:0:0
F2	16:2:2
F3	12:4:4
F4	10:5:5

The H_4DHTP solution was then added drop-wise to the magnesium acetate solution, under stirring, to avoid rapid precipitation. The mixed solutions were then immediately transferred to a 45 ml Parr reaction vessel with a Teflon liner. The sealed vessel was then placed into an oven at 125 °C for 6 h. After solvothermal synthesis, crystal samples were washed with 25 ml of DMF three times over 48 h, followed by washing with 25 ml of methanol three times over 6 days, the samples were then allowed to dry at ambient conditions before XRD and SEM analysis. In order to calculate the crystal yield of each formulation the mass of crystals recovered from after synthesis and drying in a vacuum oven at 150 °C was measured. The crystal yield was calculated based on the starting mass of H_4DHTP in the reaction solution, assuming a chemical formula of $Mg_2(DHTP)$ for Mg-MOF-74 (Equation 1). DTHP constitutes 80% of Mg-MOF-74.

$$Yield\ (\%) = [(\ M_{MOF} \times 0.8)/M_{DTHP}\ ] \times 100 \qquad 1$$

Where M_{MOF} is the mass of Mg-MOF-74 powder and M_{DTHP} is the mass of the deprotonated H_4DTHP originally dissolved in solution.

2.3 Mg-MOF-74 Film Synthesis

Tubular alumina porous supports (11-mm OD, 7-mm ID) supplied by Inopor GmbH were used as substrates for the growth of the Mg-MOF-74 films. The tubes consisted of 200 nm membrane layers, supported by more continually more porous layers beneath. Lengths of 2

cm and 6 cm were chosen for characterisation and testing respectively. The 6 cm long supports were glazing each end to provide an impenetrable seal during gas permeation tests. Before film synthesis, the supports were submerged in DI water and placed in an oven at 90 °C for 10 minutes, and then dried in an oven at 125 °C for 5 minutes, and wrapped in Teflon to ensure growth only occurred on the 200 nm pore layer.

The films were fabricated using the identical metal/ligand concentrations and solvent ratios as for the crystal syntheses at a temperature of 125 °C, except 30 ml solutions were used for 6 cm long substrates. For film fabrication, the synthesis time ranged from 1-24h. The substrates were placed directly in stainless-steel reaction vessels with Teflon liners into which the reaction solution was previously poured in. Powder crystal samples were also collected from bottom of the vessel when possible; washed and dried using the same procedure, as previously described for crystals. The films were then washed for washed with 25 ml of DMF over 12 h, followed by washing with methanol three times over 24 h, and then dried in air at room temperature for 24 h. For each solvent formulation 2 MOF films were fabricated, while 2 membranes each were fabricated using formulations F2 and F3.

2.4 Material Characterisation

The X-ray diffraction (XRD) patterns for both crystal and film samples were acquired at room temperature using a Bruker D8 Advance diffractometer. The data was collected over 3–20° angular range in 2θ in continuous scan mode using a step size and time of 0.02° and 4 s, respectively. Scanning Electron Microscopy (Phillips XL30) was carried out on crystal and film samples in order to determine the Mg-MOF-74 crystal morphology, size and film thickness. Samples were coated with platinum using a sputter coater in order to make the samples conductive. Analyses were conducted at 10 kV. BET surface areas of crystal samples were determined using a Micromeritics, TriStar II 3020, Norcross, GA gas adsorption analyser.

2.5 Single Gas Permeation Measurements

Single gas carbon dioxide and methane permeances were measured at room temperature in a flow system (**Figure 1**). The pressure drop across the membrane was maintained at 2 bar while both feed and permeate pressures were controlled with back pressure regulators. The feed flow rate was 5 cm^3 s^{-1} (standard conditions) controlled by mass flow controllers. Permeate fluxes were measured with mass flow meters. The membranes were sealed in a stainless-steel module with silicone O-rings.

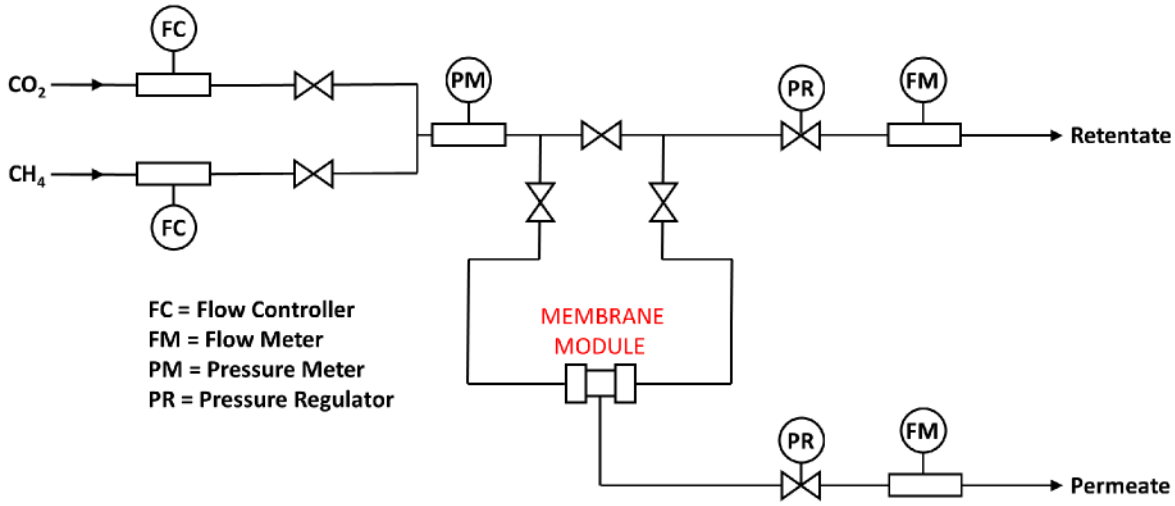

Figure 1: Gas separation rig schematic. CO_2 and CH_4 flowrate are controlled by individual flow controllers (FC). The system pressure is set by the retentate line pressure regulator (PR), while the permeate line pressure regulator is set to atmospheric pressure. The permeance of membranes are calculated using the flowrates measured on the flow meter (FM) on the permeate line.

3. Results and Discussions

3.1 Controlling Mg-MOF-74 Particle Size

Figure 2 shows X-ray diffraction pattern of Mg-MOF-74 crystals produced in this study after solvent exchange in methanol and drying at room temperature. The formation of Mg-MOF-74 was confirmed by the presence of the characteristic peaks at 6.7°, 11.7° and 18° of MOF-74 in each XRD pattern[21,31]. In addition, the broad peaks observed in XRD pattern for the synthesis with DMF only (F1) suggests that nano-crystals are produced. The size of the crystals from formulation F1 (DMF-only) formed after 6 h at 125 °C was calculated as 8.0 nm, showing good agreement with previously report[38].

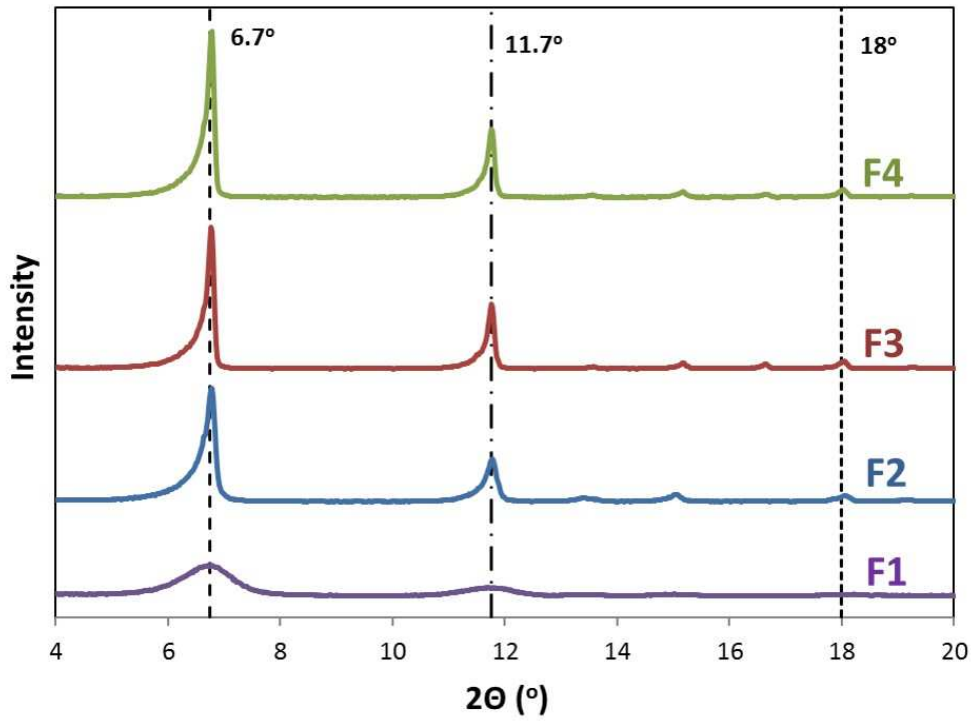

Figure 2: X-ray diffraction patterns of Mg-MOF-74 crystals formed after 6 hours at 125 °C with formulations F1-4. The dashed lines refer to the positions of the most prominent characteristic Mg-MOF-74 peaks (6.7°, 11.7° and 18°)

When the volume of water and ethanol was increased in the synthesis solutions (from F1 to F4) the intensity of the characteristic XRD peaks (6.7° and 11.7°) for Mg-MOF-74 increased and sharper peaks were obtained. Using the Scherrer equation[39] the average 'calculated' crystal size was estimated, as shown in **Table 2** including the full width at half maximum (FWHM) values of peaks at 6.7° and 11.7°. As the FWHM value decreases an associated increase in predicted crystal size is observed.

Table 2: Mg-MOF-74 crystal sizes calculated by Scherrer Equation as a function of solvent compositions (Synthesis at 125 °C for 6 hours).

Formulation	Angle (°)	FWHM (°)	'Calculated' Crystal Diameter (nm)
F1	6.7 11.7	1.02 1.00	8.0 ± 0.2
F2	6.7 11.7	0.23 0.24	34.2 ± 1.0
F3	6.7 11.7	0.16 0.16	49.5 ± 0.7
F4	6.7 11.7	0.16 0.17	49.7 ± 1.0

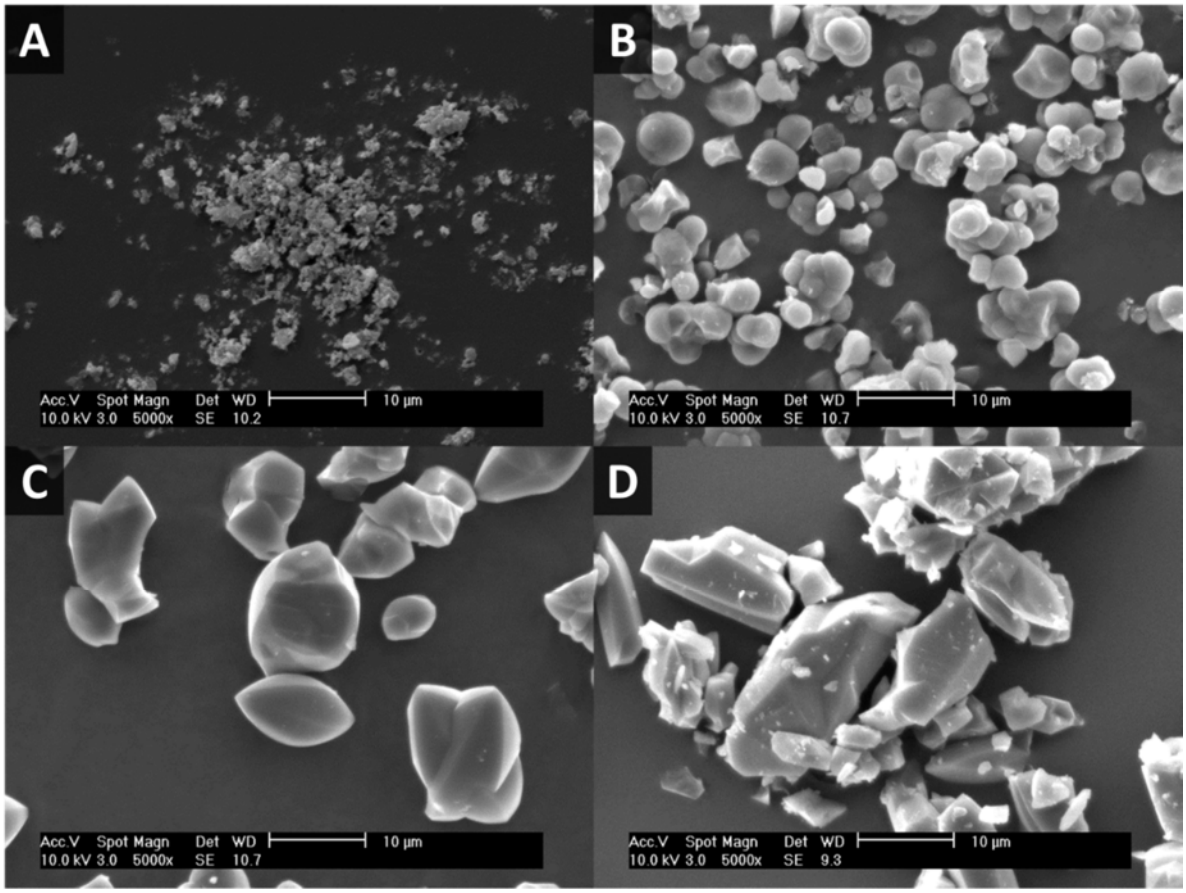

Figure 3: Scanning electron microscopy images of Mg-MOF-74 crystals at x5000 magnification for (A) F1, (B) F2, (C) F3 & (D) F4 for 6 h synthesis at 125 °C. For further magnified image of the F1 crystals see Figure S1 in the supplementary information in.

Scanning Electron Microscopy was used to validate the crystal sizes calculated using the Scherrer equation, and also determine the crystal morphologies (**Figure 3)**. The Mg-MOF-74 crystals increased in size as the ratio of water and ethanol in the reagent solution increased (from F1 - DMF only to F4 - where half the reagent solution was water and ethanol). The crystals formed using only DMF (F1), appear as agglomerated nano-scale crystals, as predicted by the Scherrer equation calculations. A magnified image Mg-MOF-74 crystals from of the formulation F1 is shown in the supplementary information in **Figure S1**. The other Mg-MOF-74 particles are on the micron scale, over 2 orders of magnitude larger than the calculations in **Table 2** as the Scherrer equation is only valid for particles up to 200 nm. The particles' sizes range from 1 to 5 µm for formulation F2, 5 to 10 µm for formulation F3 (and 10 to 20 µm for formulation F4.

The crystal shape also appears to change with increasing water and ethanol content. The morphology of the nano-scale crystals (formed using only DMF-F1) is difficult to elucidate due to the small size of the crystals and particle agglomeration (**Figure 3A**). The SEM images in **Figure 3** show that as the water/ethanol content in the synthesis solution is increased the crystals form with with more defined facets and edges. The Mg-MOF-74 crystals formed using formulation F2 (DMF:water:ethanol ratio = 16:2:2) are spherical in shape, with no defined facets. As the DMF:water:ethanol ratio is changed to 12:4:4 (F3) the crystal shape becomes more defined and tetragonal. The aspect ratio of the crystals

appears to still be 1:1:1 in the x:y:z directions, whilst there is evidence of elongation of some of the crystals. The elongation and shape change continues as the ethanol and water content is increased to half the volume of the reaction solution cumulatively. The crystals formed using formulation F4 are more than twice as long in the z direction as the x and y coordinates, leading to the formation of long column like tetragonal/hexagonal crystals that easily break apart. A similar change in crystal size and shape is observed with NH_2-MIL-53 crystals as the water volume in the reaction solution is increased[40]. Cheng *et al.* suggest smaller NH_2-MIL-53 crystal sizes occur due to rapid nucleation attributed to fast deprotonation of the organic linker in higher pH in DMF environments.

The change in the crystal size and shape with shifting solvent composition could be due to the solubility of H_4DHTP in the different solvents. The ligand is soluble in DMF, but additives such as sodium hydroxide are required to dissolve it in water. The Hildebrand solubility parameters were calculated for DMF, ethanol and water are 12.2, 12.9 and 23.5 $cal^{1/2}\,cm^{-3/2}$ respectively[41]. The Hildebrand solubility parameter of a solvent mixture was calculated by a volume adjusted average[42]. The values of the synthesis solutions F1-4 are shown in **Table 4**, alongside the calculated Hildebrand solubility parameter for H_4DHTP.

Table 4: Hildebrand Solubility Parameters for H_4DHTP and solvents

Solvent	**Hildebrand Solubility Parameter ($cal^{1/2}\,cm^{-3/2}$)**
H_4DHTP	12.7
F1	12.2
F2	13.4
F3	14.6
F4	15.2

Molecules with similar Hildebrand solubility parameters are more readily miscible. It can be seen that F1 has the closest Hildebrand solubility parameter to H_4DHTP. Suggesting that the ligand more readily dissolved in the pure DMF solution. As with NH_2-MIL-53, rapid ligand dissolution could be the cause of the small crystals obtained using formulation F1, due to rapid crystal nucleation. As the water and ethanol fraction in the mixture is increased the solubility of the ligand decreases, lowering the rate of nucleation, leading to the formation of larger crystals.

As the volume of water and ethanol in the reaction solution was increased the yield of crystals recovered decreased significantly (see **Table 3**). For DMF/water/ethanol mixtures the yields of Mg-MOF-74 decreased as the volume of DMF was reduced in the reaction solution. Previous investigations reported that Zn-MOF-74 yields increase in water/ethanol solutions with high ratios of water[33].

Table 3: Mg-MOF-74 crystal yield for synthesis solutions after 6 hours at 125 °C

Solvent formulation	**Yield (%)**
F1	100
F2	92
F3	58
F4	16

The relationship between crystal yield and the water and ethanol content is further evidence that changing the solvent mixture effects the rate of crystal nucleation, and thus the final crystal size. High nucleation rates for formulation F1 (DMF only) leads to obtaining a high yield of nano-sized crystals. As the water and ethanol volume in the synthesis solution is increased the nucleation rate reduces, producing less crystals, while the growth rate of Mg-MOF-74 at 125 °C is sufficiently high enough to allow those crystals that do form to grow larger.

3.2 Controlling Mg-MOF-74 Film Thickness

Scanning electron microscopy images of the alumina substrate and MOF film synthesized for 20 h (F1) are shown in **Figure 4**. The average pore size of alumina substrate was 200 nm (**Figure 4A**). **Figure 4B** shows a thin patch of material on the alumina surface, while the pores of the alumina substrate mostly remain visible elsewhere. Further images of the alumina surface after synthesis using formulation F1 are shown in the supplementary information (**Figure S5**). Using only DMF (F1), the crystals formed have a diameter of around 8 nm as reported by Díaz-García et al.[38] (confirmed with the Scherrer equation) and are prone to agglomeration, as can also be seen in **Figure S1**. The nano-sized particles may not readily attach to the surface of the alumina substrate, most likely because the crystals are much smaller than alumina substrate pores (200 nm). The patch of material on the surface of the film in **Figure 4B** may be due to Mg-MOF-74 crystal agglomeration, or precipitation of the organic ligand (H_4DHTP) on the alumina surface.

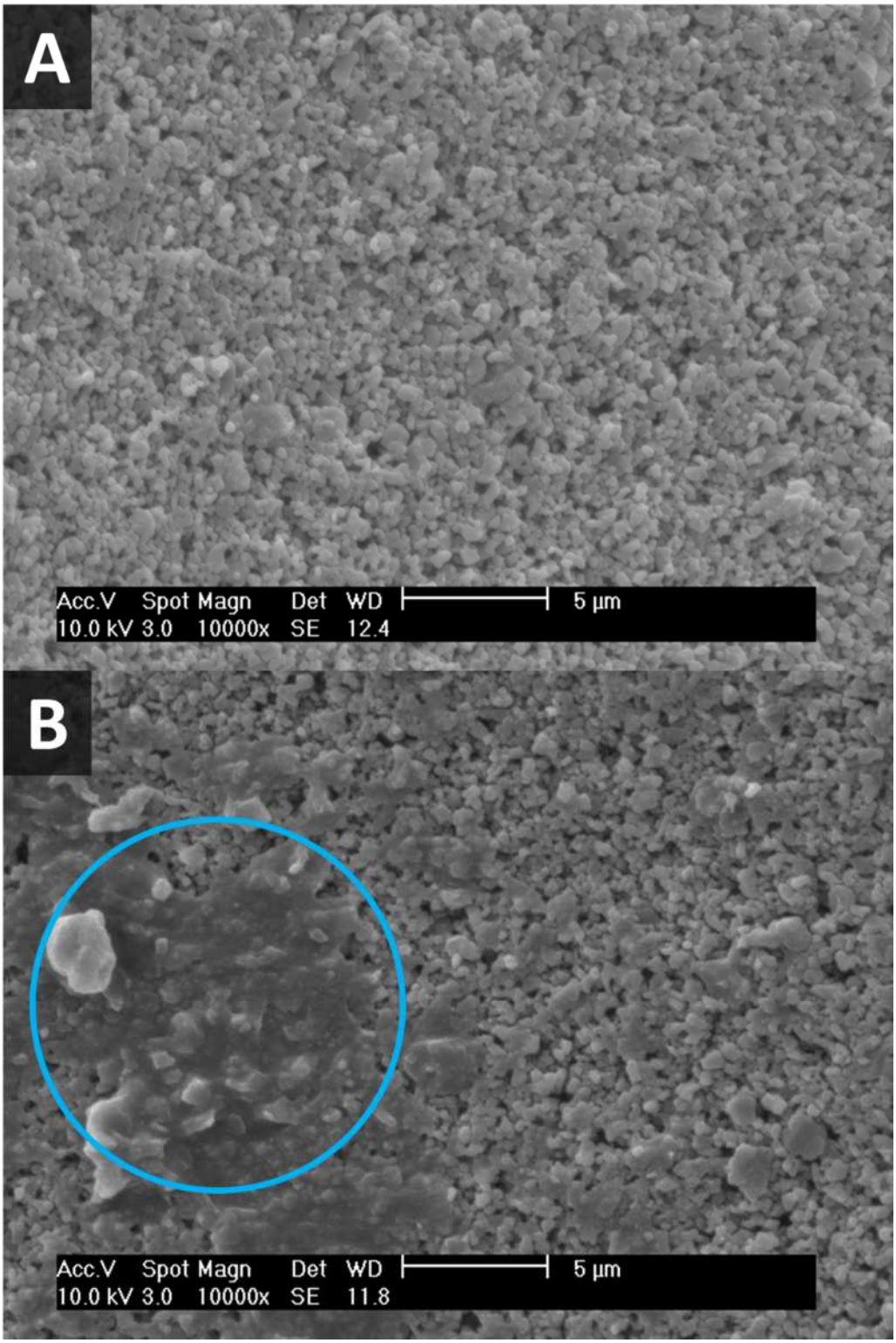

Figure 4: Surface SEM images of (A) the alumina substrate and (B) a thin patch of unidentified material on alumina surface (encircled) formed submerging an alumina substrate in a formulation F1 reaction mixture for 20 h at 125 °C.

X-ray diffraction patterns for the powder and film samples synthesised using F1 (only DMF) for 20 h are shown in **Figure 5**. None of the characteristic peaks associated with Mg-MOF-

74 are present on the surface for the film sample, confirming that there is no/very low presence of Mg-MOF-74 material on the surface of the alumina substrate.

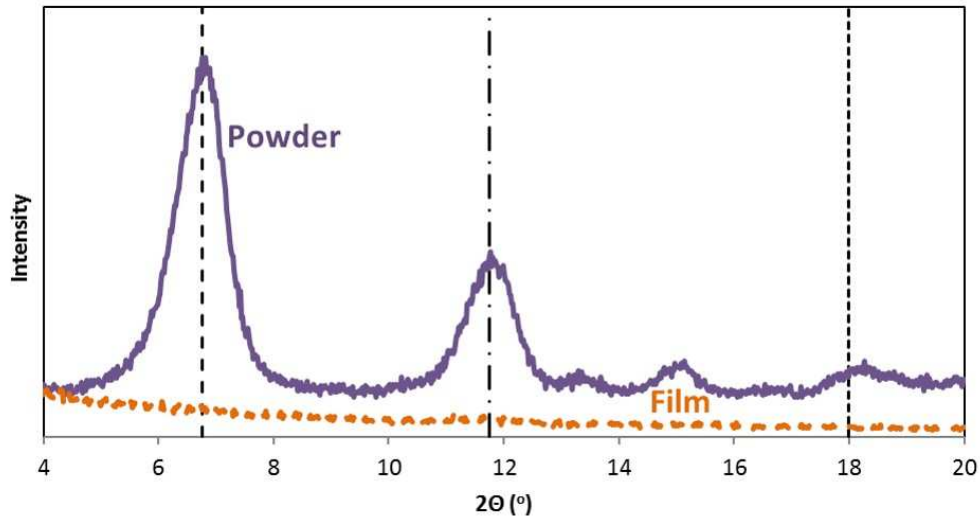

Figure 5: XRD patterns of Mg-MOF-74 powder and film synthesized using F1 for 20 h at 125 ˚C. The dashed lines refer to the positions of the most prominent characteristic Mg-MOF-74 peaks (6.7°, 11.7° and 18°)

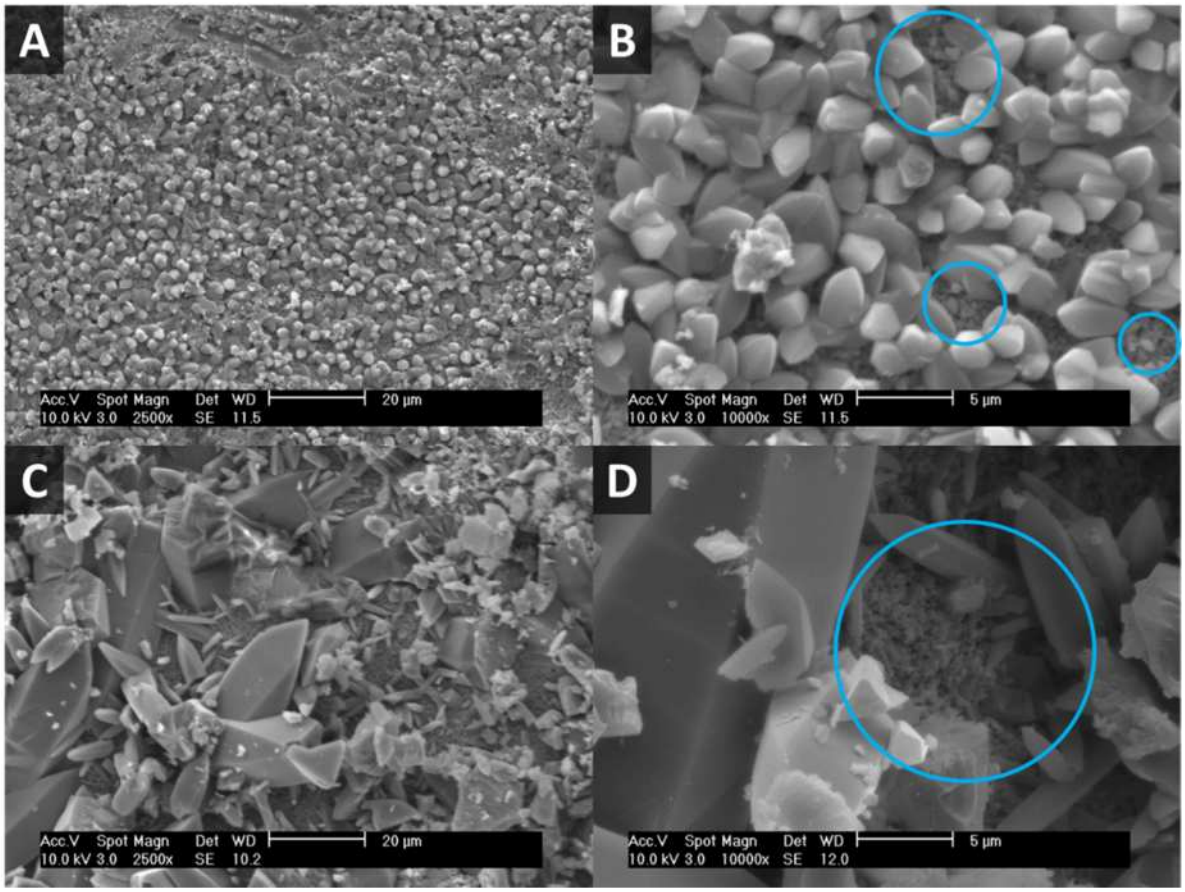

Figure 6: SEM images of film surfaces from F4 for 1 h synthesis with magnification of (A) x2500; (B) x10000; and for 24 h synthesis with magnification of (C) x2500 and (D) x10000. The blue circles show the alumina substrate between Mg-MOF-74 crystals.

In order to produce crystals that were large enough to adhere to the surface of the alumina substrate, synthesis formulations containing water and ethanol were used to produce larger particles. **Figure 6** shows SEM images of the films formed after 1 and 24 h using formulation F4, for which half the solution was water and ethanol. After 1 h, the observed crystals were ~ 1 μm in diameter, and tetragonal in shape. **Figure 6B** shows that after 1 h of synthesis a coating of Mg-MOF-74 is attached to the alumina substrate surface. However, the crystals are not well intergrown and patches of alumina substrate are seen underneath gaps between some of the crystals. When the synthesis time was increased from 1 h to 24 h the size of the crystals increased beyond 20 microns in length, whilst this increase in crystal size did not lead to the fabrication of a defect free film of crystals as gaps between crystals are observed (**Figure 6D**). The presence of a Mg-MOF-74 film was also confirmed by XRD pattern, as shown in **Figure 7.**

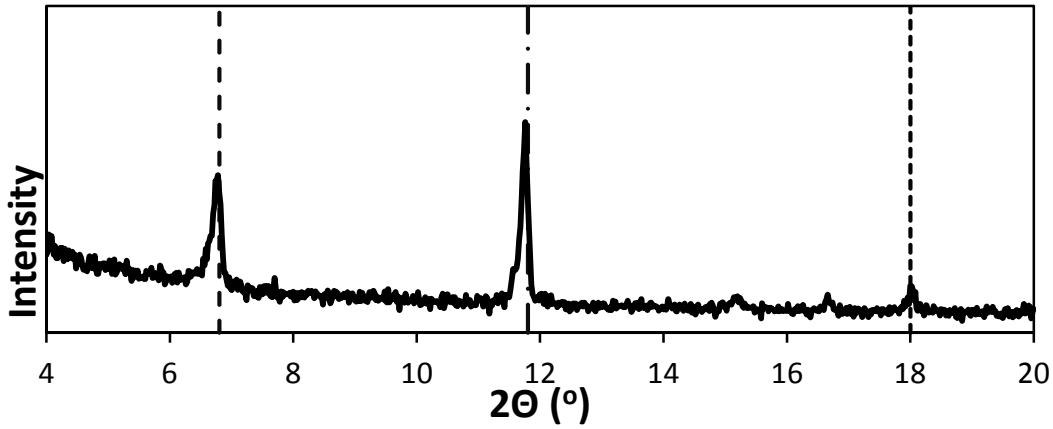

Figure 7: XRD pattern for Mg-MOF-74 film synthesised on an alumina substrate using formulation F4 for 24 hours at 125 °C. The dashed lines refer to the positions of the most prominent characteristic Mg-MOF-74 peaks (6.7°, 11.7° and 18°)

Mg-MOF-74 crystals were also grown on an alumina substrate using formulation F4 at 125 °C for 2.5 hours (see SI, **Figure S6**). The morphology of the films after 2.5 and 24 h of synthesis are similar, suggesting that the crystals size reaches a maximum (approximately 25 microns) between 1 and 2.5 h of synthesis. Those crystals may rapidly detach from the alumina substrate during synthesis, inhibiting the ability to produce a continuous film on the support surface (**Figure 6**). Due to the size and shape of the crystals (25 μm), the crystals have high individual masses, yet only a small area of the crystal surface can attach to the alumina. Larger crystals that are not well intergrown could be more likely to break off the alumina substrate. The low yield of Mg-MOF-74 using formulation F4 (**Table 3**) may also contributed to the poor coverage of crystals on the alumina surface. The low nucleation rate using this formulation is likely the cause of the presence of bare alumina between Mg-MOF-74 crystals on the substrate. In order to improve growth on the substrate, solvent formulations F2 and F3, which lead to the growth of smaller crystals with higher yields, were chosen for membrane syntheses.

Figure 8 shows the surface and cross-sectional SEM images of films formed using synthesis solutions F2 (DMF:water:ethanol ratio = 16:2:2) & F3 (12:4:4) with 2.5 h of synthesis. Images of the film surfaces show that well intergrown films of Mg-MOF-74 were grown after a synthesis time of just 2.5 hours. Coverage of Mg-MOF-74 on the alumina substrate was improved using solvent formulations F2 and F3 as compared to formulations F1 and F4. Formulations F2 and F3 contain intermediate amounts of water and ethanol between the extremes of F1 (DMF only) and F4 (in which half the solution is water/ethanol).

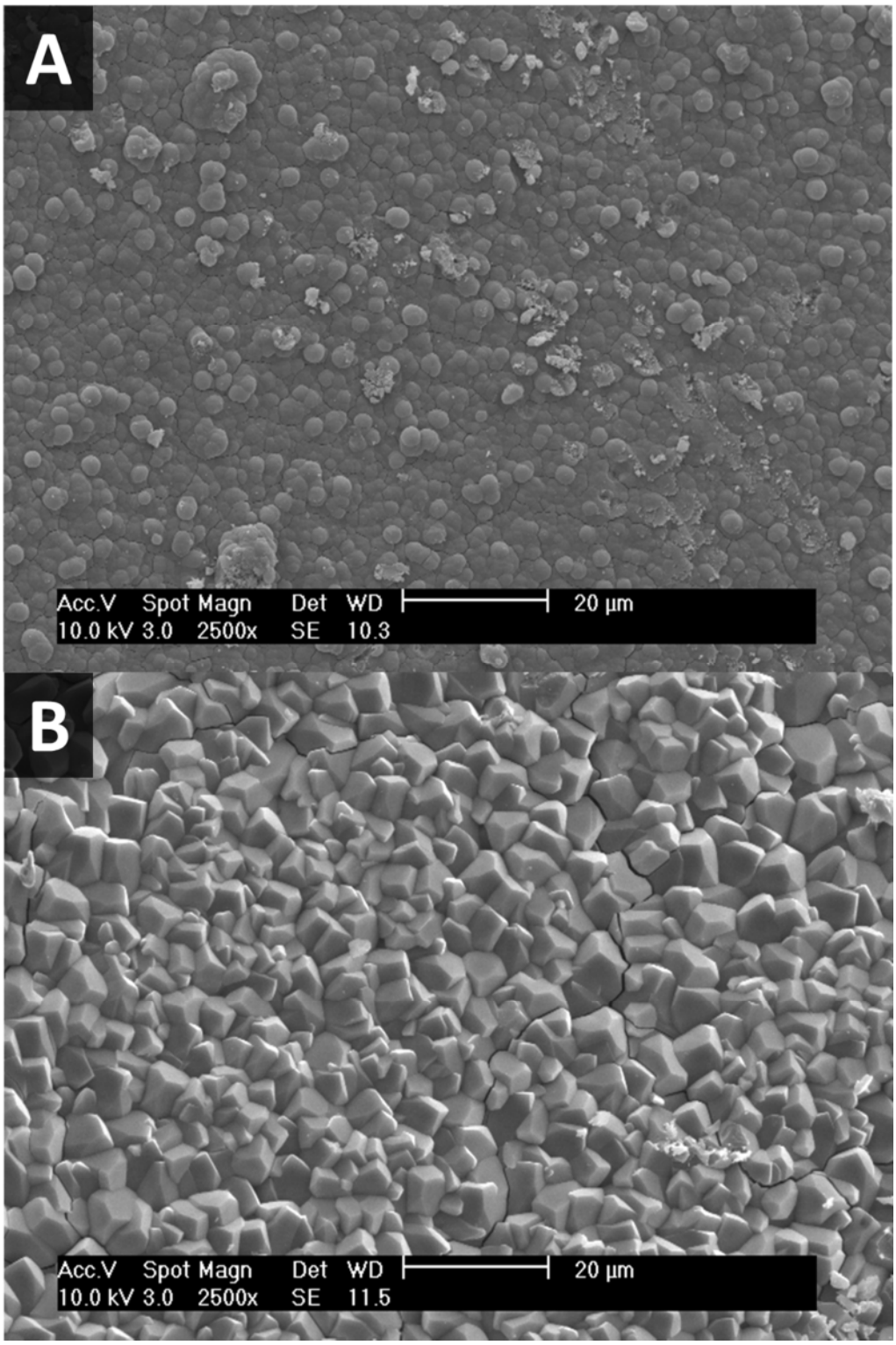

Figure 8: SEM images of the surface of the films formed using (A) F2 for 2.5 h and (B) F3 for 2.5 h. [Magnification x2500]

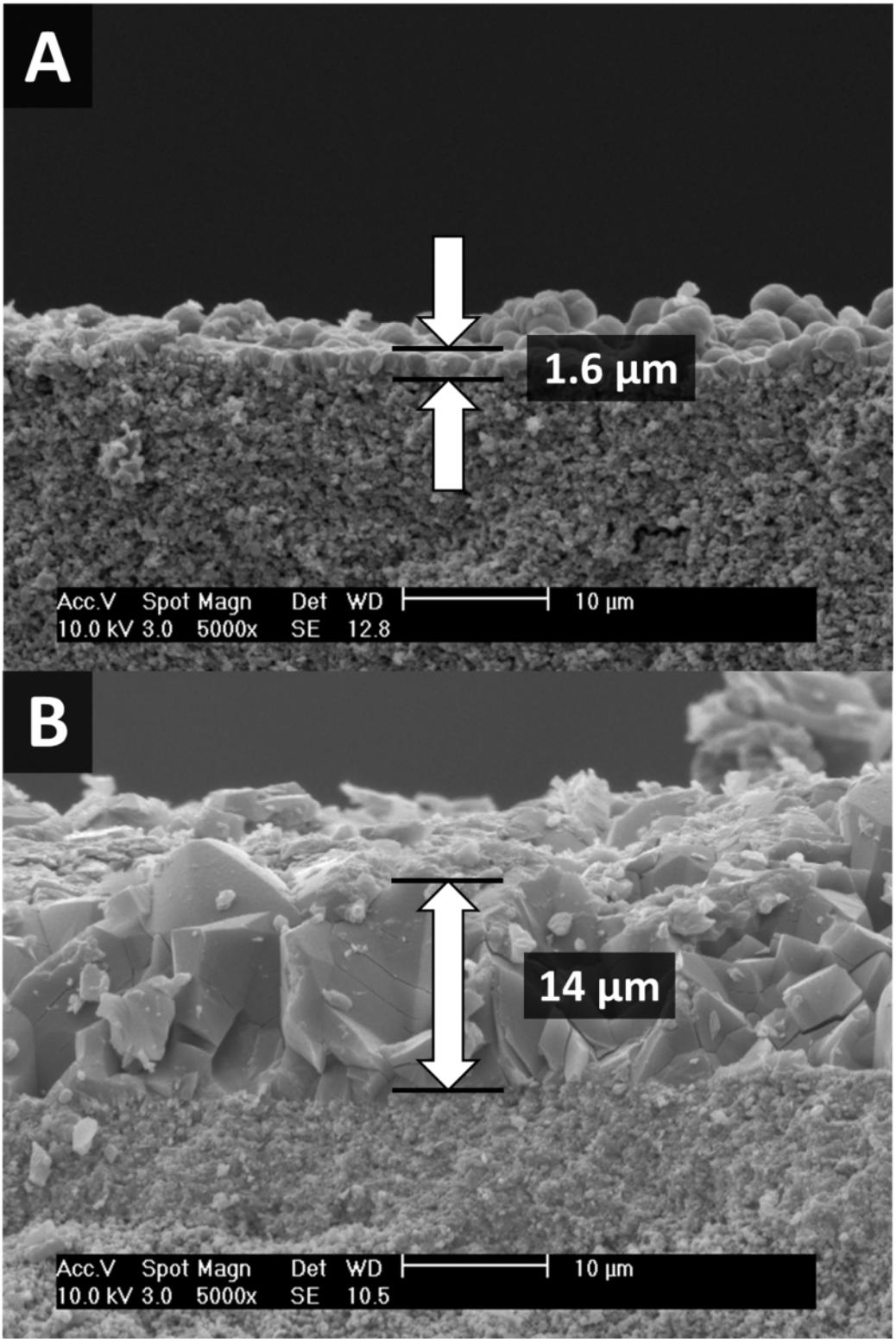

Figure 9: SEM images of the cross-section of the films formed using (A) F2 for 2.5 and (B) F3 for 2.5 h. [Magnification x5000]

The crystals grown using formulations F2 and F3 are larger than the pores of the alumina substrate allowing the crystals to attach to the substrate surface. Higher nucleation rates of formulation F2 and F3 above F4 may allow the formation of continuous Mg-MOF-74 films as there are no visible gaps between the crystals (**Figure 8A & 8B**). The 1 µm spherical particles for F2 and 3-5 µm crystals with low aspect ratios in the x:y:z directions for F3, may suggest that the crystals readily remain on the support surface, and can easily fuse during growth. **Figure 9A** shows the cross-sectional area of the film synthesized by formulation F2 for 2.5 h. The film layers are ~ 1.6 and 14 µm thick for F2 and F3, respectively. The thinnest previous M-MOF-74 membranes had a thickness of 10 µm, making the film formed using formulation F2 over 6 times thinner than previous membranes.

Figure 10 shows the XRD patterns for the films synthesised using F2 and F3 after 2.5 h. The intensity of the characteristic peaks at 6.7°, 11.7° and 18° for the film formed using F3 was higher than those for the film formed using F2. This is likely due to both the increase in film thickness and crystal size obtained using F3.

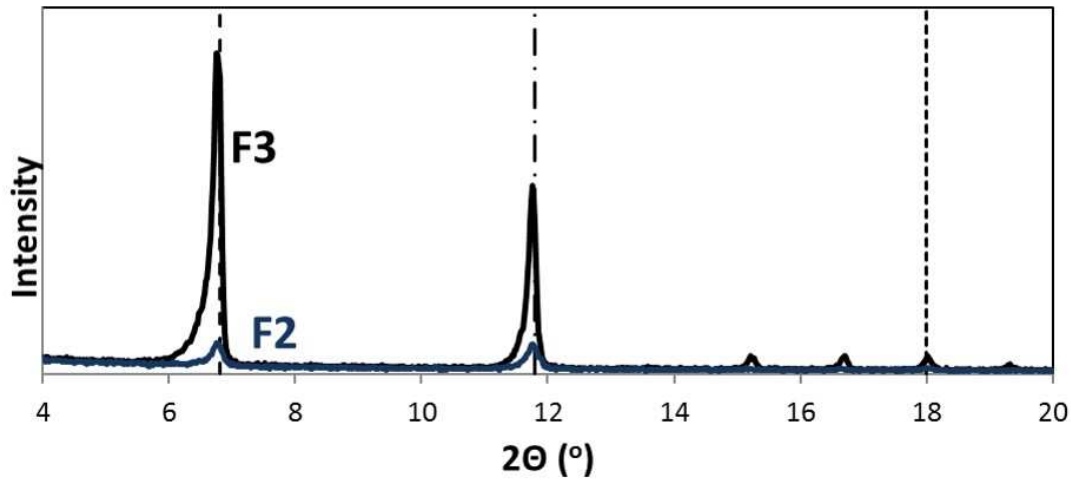

Figure 10: The XRD patterns of the films synthesised using formulation F2 and F3 for 2.5 hours. The dashed lines refer to the positions of the most prominent characteristic Mg-MOF-74 peaks (6.7°, 11.7° and 18°)

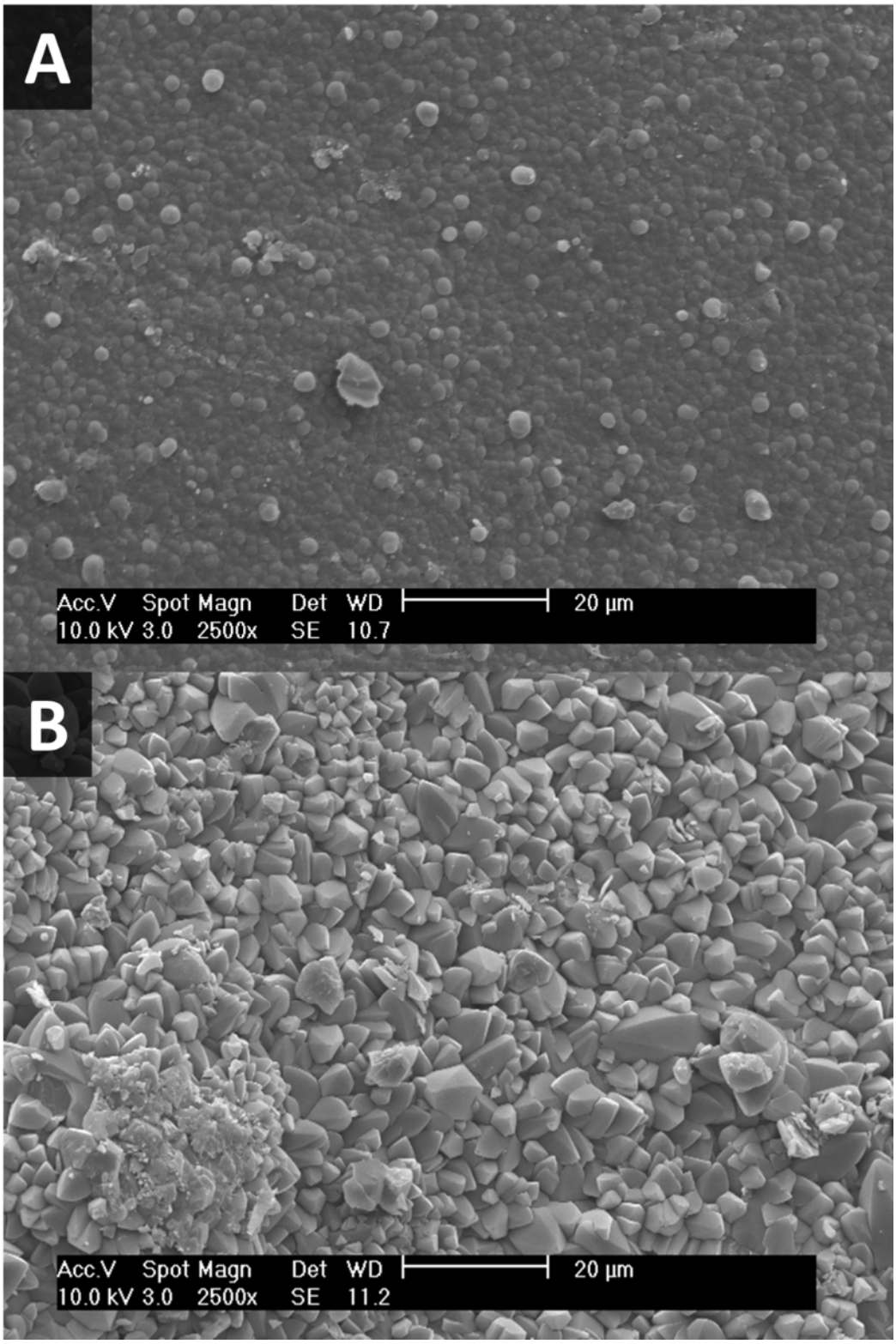

Figure 11: SEM images of the surface of the films formed using (A) F2 for 6 hours and (B) F3 for 6 hours.

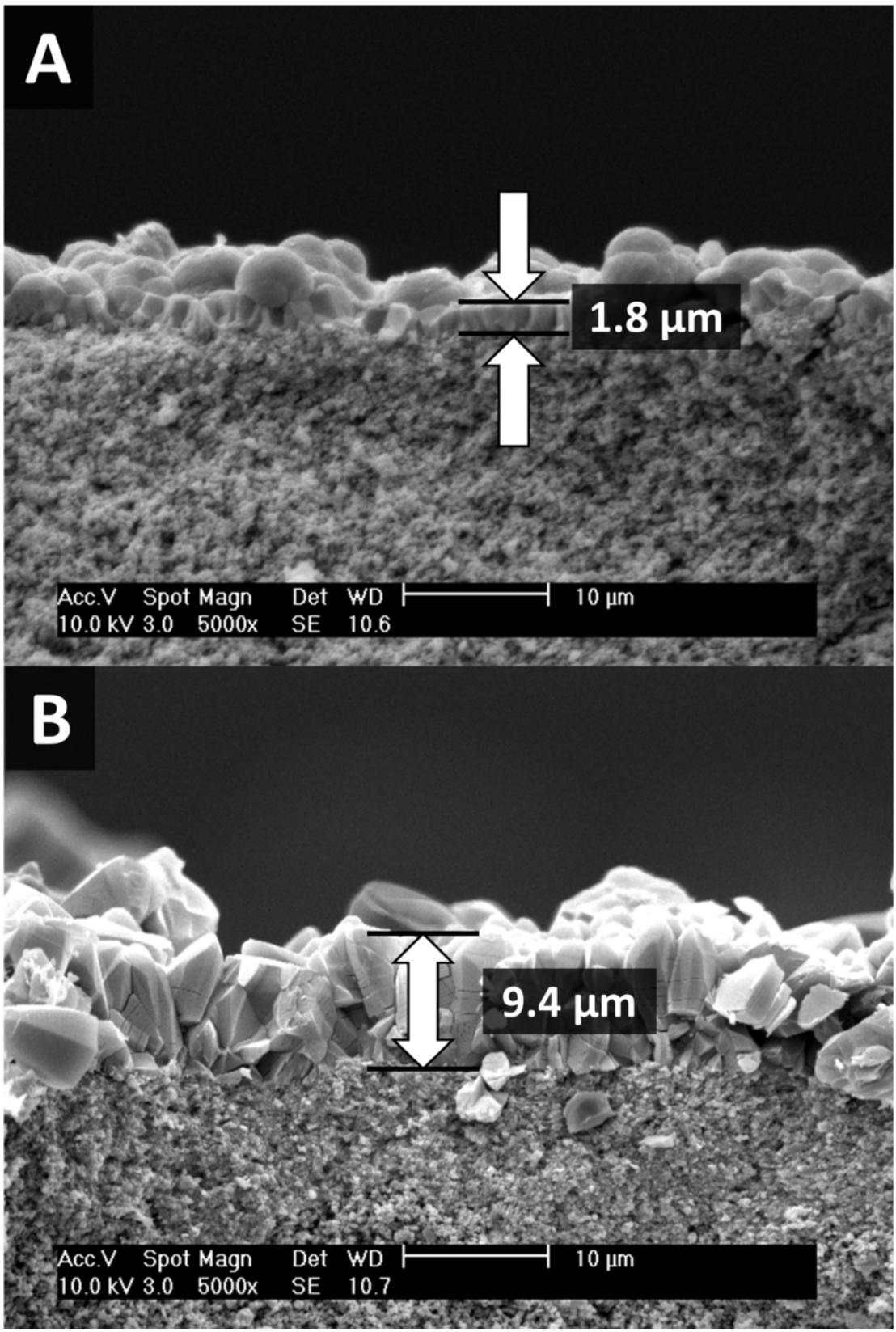

Figure 12: SEM images of the cross-section of the films formed using (A) F2 for 6 hours and (B) F3 for 6 hours.

The effect of time on film thickness and defects was also determined by increasing the reaction time. **Figures 11** and **12** show SEM images of Mg-MOF-74 films formed using F2 and F3 after 6 hours of synthesis at 125 °C. The observed morphologies of the F2 films and the crystals did not change whether 2.5 h (**Figure 8A & 9A**) or 6 h (**Figure 11A & 12A**) syntheses was employed. The thickness of the F2 film formed after 6 h is roughly 1.8 µm (**Figure 12A**). However, using formulation F3 for 6 h synthesis a thinner film (10 µm) was obtained compared to 2.5 h of synthesis (14 µm). The crystal morphology also changed from the cubic-like crystals found after 2.5 h to oriented column-like hexagonal/tetragonal crystals. The difference in the crystal morphology and film thickness with increased synthesis time is counterintuitive to what would be expected, with the change in thickness likely to affect permeation of gases.

3.4 Single Gas Permeation Measurements

Table 5 shows single gas CO_2 permeance and ideal CO_2/CH_4 selectivity for M-MOF-74 membranes. Permeation tests were carried out using formulations F2 and F3 (2.5 h) as these syntheses yielded to continuous films. Due to the lack of a clear relationship between activation conditions and the loss of BET area of the Mg-MOF-74 crystals, the films were dried in ambient conditions only before testing (see supplementary information).

Table 5: Single gas permeation results of membranes at 1 bar

M-MOF-74 Membrane	**CO_2 Permeance x10^{-8} (mol m^{-2} s^{-1} Pa^{-1})**	**Ideal CO_2/CH_4 Selectivity**
Mg-MOF-74 (F2)	74	0.49
Mg-MOF-74 (F3)	N/A	N/A
"layer-by-layer" Ni-MOF-74[30]	0.014	0.32
amine-modified Mg-MOF-74[31]	1.1	0.5

During the tests, the membranes formed using formulation F3 could not hold pressure, and thus no permeation and selectivity data could be collected. This is likely due to formation of defects/cracks in the films at crystal interfaces, which is not visible in SEM images.

The permeance values achieved for the gases are 2 orders of magnitude higher than those achieved for previous Mg-MOF-74 membranes[31]. Due to the high affinity for CO_2 of Mg-MOF-74, adsorption studies have shown the material to be highly selective for CO_2 over CH_4[21]. However, studies of the diffusion kinetics of CH_4 and CO_2 through the MOF show that CH_4 travels through the pores 5 times faster[20]. In addition, CO_2 may not be desorbed fast enough when compared to CH_4. M-MOF-74 membranes in literature have higher CH_4 permeances than those of CO_2 suggesting that the diffusion kinetics of the gases through the MOF cages may determine the separation performance[31]. The performance of M-MOF-74 membranes must be improved to compete with other MOFs such as ZIF-8[10] (CO_2 Permeance = 2430 x10^{-8} mol m^{-2} s^{-1} Pa^{-1} and CO_2/CH_4 ideal selectivity = 5.1) and $CO_3(HCOO)_6$[16] (CO_2 permeance = 225 x10^{-8} mol m^{-2} s^{-1} Pa^{-1} and CO_2/CH_4 ideal selectivity = 5.4). Improved membrane performances could be achieved by further studying the MOF activation parameters and/or post-synthesis modification such as ligand exchange to introduce amine groups to the framework.

4. Conclusions

Through shifting the solvent composition of Mg-MOF-74 synthesis solutions the size of the crystals formed can be tailored. Synthesis solutions containing increased ratios of water and ethanol lead to formation of larger crystals, but with a subsequent reduction in yield. Changes in the nucleation rate of crystals are thought to influence the final crystal size and yield, with high nucleation rates for DMF only solutions that decrease with increasing water/ethanol content.

Nano-scale crystals produced using only DMF as solvent (F1) failed to produce viable films on the surface of alumina substrates. The F2 synthesis solution containing a solvent ratio of 16:2:2 for DMF, water and ethanol respectively, led to the formation of 1-2 µm Mg-MOF-74 films, an order of magnitude thinner than previously achievable for M-MOF-74 films. Thicker films (10-20 µm) were synthesised in 2.5 and/or 6 h by further increasing the water and ethanol content of the synthesis solution (F3, DMF:water:ethanol ratio = 12:4:4). When the water and ethanol content was increased to half the volume of the synthesis solution, the formation of continuous defect free films with well intergrown crystals was not possible.

This paper demonstrates for the first time a controllable methodology with which to produce Mg-MOF-74 membranes of different thicknesses. In addition, these membranes can be produced in only 2.5 hours without seeding. The synthesis is significantly faster than the growth of previous M-MOF-74 films (>24 h). Improvements are needed to the post-synthesis activation of the MOF pores in order maximise the selectivity of the membranes for mixed gas feeds. Future studies will also explore the effect of reaction solution concentration on the size and shape of Mg-MOF-74 crystals, the crystal orientation and thickness of membranes, as well as extending the one-step film fabrication methodology to other members of the M-MOF-74 series.

Acknowledgements

The authors would like to acknowledge financial support for this work from the University of Nottingham, Faculty of Engineering, Dean of Engineering Prize. The authors would also like to thank Ms. Yipei Chen and Professor Edward Lester for assistance with BET surface area analysis.

References

(1) Fang, Q.; Sculley, J.; Zhou, H.-C. J.; Zhu, G. 5.01 - Porous Metal–Organic Frameworks. In *Comprehensive Nanoscience and Technology*; Andrews, D. L., Scholes, G. D., Wiederrecht, G. P., Eds.; Academic Press: Amsterdam, 2011; pp 1–20.

(2) Qiu, S.; Xue, M.; Zhu, G. Metal–organic Framework Membranes: From Synthesis to Separation Application. *Chem. Soc. Rev.* **2014**, *43* (16), 6116–6140.

(3) Shah, M.; McCarthy, M. C.; Sachdeva, S.; Lee, A. K.; Jeong, H.-K. Current Status of Metal-Organic Framework Membranes for Gas Separations: Promises and Challenges. *Ind. Eng. Chem. Res.* **2011**, *51* (5), 2179–2199.

(4) Tanaka, S.; Fujita, K.; Miyake, Y.; Miyamoto, M.; Hasegawa, Y.; Makino, T.; Van der Perre, S.; Cousin Saint Remi, J.; Van Assche, T.; Baron, G. V.; Denayer, J. F. M. Adsorption and Diffusion Phenomena in Crystal Size Engineered ZIF-8 MOF. *J. Phys. Chem. C* **2015**, *119* (51), 28430–28439.

(5) V. McGuire, C.; S. Forgan, R. The Surface Chemistry of Metal–organic Frameworks. *Chem. Commun.* **2015**, *51* (25), 5199–5217.

(6) Nordin, N. a. H. M.; Ismail, A. F.; Mustafa, A.; Murali, R. S.; Matsuura, T. The Impact of ZIF-8 Particle Size and Heat Treatment on CO2/CH4 Separation Using Asymmetric Mixed Matrix Membrane. *RSC Adv.* **2014**, *4* (94), 52530–52541.
(7) Sabetghadam, A.; Seoane, B.; Keskin, D.; Duim, N.; Rodenas, T.; Shahid, S.; Sorribas, S.; Guillouzer, C. L.; Clet, G.; Tellez, C.; Daturi, M.; Coronas, J.; Kapteijn, F.; Gascon, J. Metal Organic Framework Crystals in Mixed-Matrix Membranes: Impact of the Filler Morphology on the Gas Separation Performance. *Adv. Funct. Mater.* **2016**, *26* (18), 3154–3163.
(8) Shahid, S.; Nijmeijer, K.; Nehache, S.; Vankelecom, I.; Deratani, A.; Quemener, D. MOF-Mixed Matrix Membranes: Precise Dispersion of MOF Particles with Better Compatibility via a Particle Fusion Approach for Enhanced Gas Separation Properties. *J. Membr. Sci.* **2015**, *492*, 21–31.
(9) Knebel, A.; Friebe, S.; Bigall, N. C.; Benzaqui, M.; Serre, C.; Caro, J. Comparative Study of MIL-96(Al) as Continuous Metal–Organic Frameworks Layer and Mixed-Matrix Membrane. *ACS Appl. Mater. Interfaces* **2016**, *8* (11), 7536–7544.
(10) Venna, S. R.; Carreon, M. A. Highly Permeable Zeolite Imidazolate Framework-8 Membranes for CO2/CH4 Separation. *J. Am. Chem. Soc.* **2009**, *132* (1), 76–78.
(11) Lai, L. S.; Yeong, Y. F.; Lau, K. K.; Shariff, A. M. Synthesis of Zeolitic Imidazolate Frameworks (ZIF)-8 Membrane and Its Process Optimization Study in Separation of CO2 from Natural Gas. *J. Chem. Technol. Biotechnol.* **2016**, n/a-n/a.
(12) Shamsaei, E.; Lin, X.; Low, Z.-X.; Abbasi, Z.; Hu, Y.; Liu, J. Z.; Wang, H. Aqueous Phase Synthesis of ZIF-8 Membrane with Controllable Location on an Asymmetrically Porous Polymer Substrate. *ACS Appl. Mater. Interfaces* **2016**, *8* (9), 6236–6244.
(13) Liu, Y.; Ng, Z.; Khan, E. A.; Jeong, H.-K.; Ching, C.; Lai, Z. Synthesis of Continuous MOF-5 Membranes on Porous α-Alumina Substrates. *Microporous Mesoporous Mater.* **2009**, *118* (1–3), 296–301.
(14) Guo, Y.; Mao, Y.; Hu, P.; Ying, Y.; Peng, X. Self–confined Synthesis of HKUST-1 Membranes from CuO Nanosheets at Room Temperature. *ChemistrySelect* **2016**, *1* (1), 108–113.
(15) Guerrero, V. V.; Yoo, Y.; McCarthy, M. C.; Jeong, H.-K. HKUST-1 Membranes on Porous Supports Using Secondary Growth. *J. Mater. Chem.* **2010**, *20* (19), 3938–3943.
(16) Zou, X.; Zhang, F.; Thomas, S.; Zhu, G.; Valtchev, V.; Mintova, S. Co3(HCOO)6 Microporous Metal-Organic Framework Membrane for Separation of CO2/CH4 Mixtures. *Chem. Weinh. Bergstr. Ger.* **2011**, *17* (43), 12076–12083.
(17) Liu, Y.; Hu, E.; Khan, E. A.; Lai, Z. Synthesis and Characterization of ZIF-69 Membranes and Separation for CO2/CO Mixture. *J. Membr. Sci.* **2010**, *353* (1–2), 36–40.
(18) Liu, Y.; Zeng, G.; Pan, Y.; Lai, Z. Synthesis of Highly c-Oriented ZIF-69 Membranes by Secondary Growth and Their Gas Permeation Properties. *J. Membr. Sci.* **2011**, *379* (1–2), 46–51.
(19) Bétard, A.; Bux, H.; Henke, S.; Zacher, D.; Caro, J.; Fischer, R. A. Fabrication of a CO2-Selective Membrane by Stepwise Liquid-Phase Deposition of an Alkylether Functionalized Pillared-Layered Metal-Organic Framework [Cu2L2P]n on a Macroporous Support. *Microporous Mesoporous Mater.* **2012**, *150*, 76–82.
(20) Bao, Z.; Yu, L.; Ren, Q.; Lu, X.; Deng, S. Adsorption of CO2 and CH4 on a Magnesium-Based Metal Organic Framework. *J. Colloid Interface Sci.* **2011**, *353* (2), 549–556.
(21) Wu, X.; Bao, Z.; Yuan, B.; Wang, J.; Sun, Y.; Luo, H.; Deng, S. Microwave Synthesis and Characterization of MOF-74 (M = Ni, Mg) for Gas Separation. *Microporous Mesoporous Mater.* **2013**, *180*, 114–122.
(22) Cho, H.-Y.; Yang, D.-A.; Kim, J.; Jeong, S.-Y.; Ahn, W.-S. CO2 Adsorption and Catalytic Application of Co-MOF-74 Synthesized by Microwave Heating. *Catal. Today* **2012**, *185* (1), 35–40.
(23) Zhang, Z.; Yao, Z.-Z.; Xiang, S.; Chen, B. Perspective of Microporous Metal–organic Frameworks for CO2 Capture and Separation. *Energy Environ. Sci.* **2014**, *7* (9), 2868–2899.

(24) Bernini, M. C.; Blanco, A. A. G.; Villarroel-Rocha, J.; Fairen-Jimenez, D.; Sapag, K.; Ramirez-Pastor, A. J.; Narda, G. E. Tuning the Target Composition of Amine-Grafted CPO-27-Mg for Capture of CO2 under Post-Combustion and Air Filtering Conditions: A Combined Experimental and Computational Study. *Dalton Trans.* **2015**, *44* (43), 18970–18982.
(25) Yang, D.-A.; Cho, H.-Y.; Kim, J.; Yang, S.-T.; Ahn, W.-S. CO2 Capture and Conversion Using Mg-MOF-74 Prepared by a Sonochemical Method. *Energy Environ. Sci.* **2012**, *5* (4), 6465–6473.
(26) Remy, T.; Peter, S. A.; Van der Perre, S.; Valvekens, P.; De Vos, D. E.; Baron, G. V.; Denayer, J. F. M. Selective Dynamic CO2 Separations on Mg-MOF-74 at Low Pressures: A Detailed Comparison with 13X. *J. Phys. Chem. C* **2013**, *117* (18), 9301–9310.
(27) Britt, D.; Furukawa, H.; Wang, B.; Glover, T. G.; Yaghi, O. M. Highly Efficient Separation of Carbon Dioxide by a Metal-Organic Framework Replete with Open Metal Sites. *Proc. Natl. Acad. Sci.* **2009**, *106* (49), 20637–20640.
(28) Kong, L.; Zou, R.; Bi, W.; Zhong, R.; Mu, W.; Liu, J.; Han, R. P. S.; Zou, R. Selective Adsorption of CO2/CH4 and CO2/N2 within a Charged Metal–organic Framework. *J. Mater. Chem. A* **2014**, *2* (42), 17771–17778.
(29) Bétard, A.; Zacher, D.; Fischer, R. A. Dense and Homogeneous Coatings of CPO-27-M Type Metal–organic Frameworks on Alumina Substrates. *CrystEngComm* **2010**, *12* (11), 3768–3772.
(30) Lee, D.-J.; Li, Q.; Kim, H.; Lee, K. Preparation of Ni-MOF-74 Membrane for CO2 Separation by Layer-by-Layer Seeding Technique. *Microporous Mesoporous Mater.* **2012**, *163*, 169–177.
(31) Wang, N.; Mundstock, A.; Liu, Y.; Huang, A.; Caro, J. Amine-Modified Mg-MOF-74/CPO-27-Mg Membrane with Enhanced H2/CO2 Separation. *Chem. Eng. Sci.* **2015**, *124*, 27–36.
(32) Haque, E.; Jhung, S. H. Synthesis of Isostructural Metal–organic Frameworks, CPO-27s, with Ultrasound, Microwave, and Conventional Heating: Effect of Synthesis Methods and Metal Ions. *Chem. Eng. J.* **2011**, *173* (3), 866–872.
(33) Morris, R. E.; Wheatley, P. S.; Warrender, S.; DUNCAN, M. Synthesis of Mofs. WO2013186542 A1, December 19, 2013.
(34) Wang, N.; Liu, T.; Shen, H.; Ji, S.; Li, J.-R.; Zhang, R. Ceramic Tubular MOF Hybrid Membrane Fabricated through in Situ Layer-by-Layer Self-Assembly for Nanofiltration. *AIChE J.* **2016**, *62* (2), 538–546.
(35) Liu, X.; Demir, N. K.; Wu, Z.; Li, K. Highly Water-Stable Zirconium Metal–Organic Framework UiO-66 Membranes Supported on Alumina Hollow Fibers for Desalination. *J. Am. Chem. Soc.* **2015**, *137* (22), 6999–7002.
(36) Brown, A. J.; Brunelli, N. A.; Eum, K.; Rashidi, F.; Johnson, J. R.; Koros, W. J.; Jones, C. W.; Nair, S. Interfacial Microfluidic Processing of Metal-Organic Framework Hollow Fiber Membranes. *Science* **2014**, *345* (6192), 72–75.
(37) Hou, J.; Sutrisna, P. D.; Zhang, Y.; Chen, V. Formation of Ultrathin, Continuous Metal–Organic Framework Membranes on Flexible Polymer Substrates. *Angew. Chem. Int. Ed.* **2016**, *55* (12), 3947–3951.
(38) Díaz-García, M.; Mayoral, Á.; Díaz, I.; Sánchez-Sánchez, M. Nanoscaled M-MOF-74 Materials Prepared at Room Temperature. *Cryst. Growth Des.* **2014**, *14* (5), 2479–2487.
(39) Holzwarth, U.; Gibson, N. The Scherrer Equation versus the "Debye-Scherrer Equation." *Nat. Nanotechnol.* **2011**, *6* (9), 534–534.
(40) Cheng, X.; Zhang, A.; Hou, K.; Liu, M.; Wang, Y.; Song, C.; Zhang, G.; Guo, X. Size- and Morphology-Controlled NH2-MIL-53(Al) Prepared in DMF–water Mixed Solvents. *Dalton Trans.* **2013**, *42* (37), 13698–13705.
(41) Burke, J. Solubility Parameters: Theory and Application. *Book Pap. Group Annu.* **1984**, *3*, 13–58.
(42) Carvalho, S. P.; Lucas, E. F.; González, G.; Spinelli, L. S. Determining Hildebrand Solubility Parameter by Ultraviolet Spectroscopy and Microcalorimetry. *J. Braz. Chem. Soc.* **2013**, *24* (12), 1998–2007.